Therapeutic Discovery

Molecular Cancer Therapeutics

Trans,*trans*,*trans*-[$Pt^{IV}(N_3)_2(OH)_2(py)(NH_3)$]: A Light-Activated Antitumor Platinum Complex That Kills Human Cancer Cells by an Apoptosis-Independent Mechanism

Aron F. Westendorf[1], Julie A. Woods[2], Katharina Korpis[1], Nicola J. Farrer[3], Luca Salassa[3], Kim Robinson[2], Virginia Appleyard[2], Karen Murray[2], Renate Grünert[1], Alastair M. Thompson[2], Peter J. Sadler[3], and Patrick J. Bednarski[1]

Abstract

Photoactivatable Pt^{IV} diazido complexes have unusual photobiologic properties. We show here that *trans*,*trans*,*trans*-[$Pt^{IV}(N_3)_2(OH)_2(py)(NH_3)$] complex 3 is a potent photoactivated cytotoxin toward human cancer cells in culture, with an average IC_{50} value in 13 cell lines of 55 ± 28 μmol/L after 30 minutes (0.12 mW/cm^2) photoactivation with UVA, although visible light was also effective. Photoactivated complex 3 was noncross-resistant to cisplatin in 3 of 4 resistant cell lines. Cell swelling but very little blebbing was seen for HL60 cells treated with irradiated complex 3. Unlike cisplatin and etoposide, both of which cause apoptosis in HL60 cells, no apoptosis was observed for UVA-activated complex 3 by the Annexin V/propidium iodide flow cytotometry assay. Changes in the levels of the autophagic proteins LC3B-II and p62 in HL60 cells treated with UVA-activated complex 3 indicate autophagy is active during cell death. In a clonogenic assay with the SISO human cervix cancer cell line, 3 inhibited colony formation when activated by UVA irradiation. Antitumor activity of complex 3 in mice bearing xenografted OE19 esophageal carcinoma tumors was photoaugmented by visible light. Insights into the novel reaction pathways of complex 3 have been obtained from $^{14}N\{^1H\}$ nuclear magnetic resonance studies, which show that photoactivation pathways can involve release of free azide in buffered solution. Density functional theory (DFT) and time-dependent DFT calculations revealed the dissociative character of singlet and triplet excited states of complex 3, which gives rise to reactive, possibly cytotoxic azidyl radicals. *Mol Cancer Ther; 11(9); 1894–904. ©2012 AACR.*

Introduction

Transition metal coordination complexes offer much scope for selective interference in biologic pathways and therefore have potential as therapeutic agents with novel modes of action (1). Their reactivities depend not only on the metal itself and its oxidation state but also on the number and nature of the coordinated ligands, and the geometry of the complex. Thus, *cis*-[$PtCl_2(NH_3)_2$] is a successful anticancer drug (cisplatin), but its *trans* isomer is inactive. The second-generation platinum drug carboplatin, [Pt(1,1-dicarboxycyclobutane)$(NH_3)_2$], is much less potent than cisplatin but has fewer side effects.

Authors' Affiliations: [1]Department of Pharmaceutical and Medicinal Chemistry, Institute of Pharmacy, University of Greifswald, Greifswald, Germany; [2]Dundee Cancer Centre, Ninewells Hospital, University of Dundee, Dundee; and [3]Department of Chemistry, University of Warwick, Gibbet Hill Road, Coventry, United Kingdom

Note: Supplementary data for this article are available at Molecular Cancer Therapeutics Online (http://mct.aacrjournals.org/).

Corresponding Author: Patrick J. Bednarski, Department of Pharmaceutical and Medicinal Chemistry, Institute of Pharmacy, University of Greifswald, F.-L.-Jahnstrasse 17, Greifswald, 17487, Germany. Phone: 49-3834-864-883; Fax: 49-3834-864-901; E-mail: bednarsk@uni-greifswald.de

doi: 10.1158/1535-7163.MCT-11-0959

We are exploring the possibility of increasing the selectivity of platinum drugs for cancer cells by the design of less toxic platinum prodrugs that can be selectively activated by light (2, 3). These are based on classically inert low-spin $5d^6$ octahedral Pt^{IV} complexes that incorporate light absorption and photodecomposition features. Particularly promising are diazido Pt^{IV} complexes, which possess intense azide-to-Pt^{IV} ligand-to-metal charge-transfer (LMCT) bands. Metal azido complexes are known to undergo a number of photochemical reactions, including metal reduction and azido radical formation (4). Initially, we based the design on *cis*-diam(m)ine systems such as *cis*,*trans*,*cis*-[$Pt(N_3)_2(OH)_2(NH_3)_2$], complex 1, in the belief that photoactivation would involve one-electron transfer from azide to Pt^{IV} and recombination of the released azido radicals to give dinitrogen as a product, along with square-planar Pt^{II} species that might react with DNA and produce similar lethal lesions (intrastrand GG cross-links) as cisplatin and carboplatin (5). Indeed, we were able to show that such reactions are possible in chemical systems (6).

Surprising was our finding that photoactivation of complex 1 (Fig. 1A) in bladder cancer cells caused unusual changes in cell morphology, including apparent destruction of the cell nuclei (7). This suggested that photoactivation can lead to novel mechanisms of cytotoxicity,

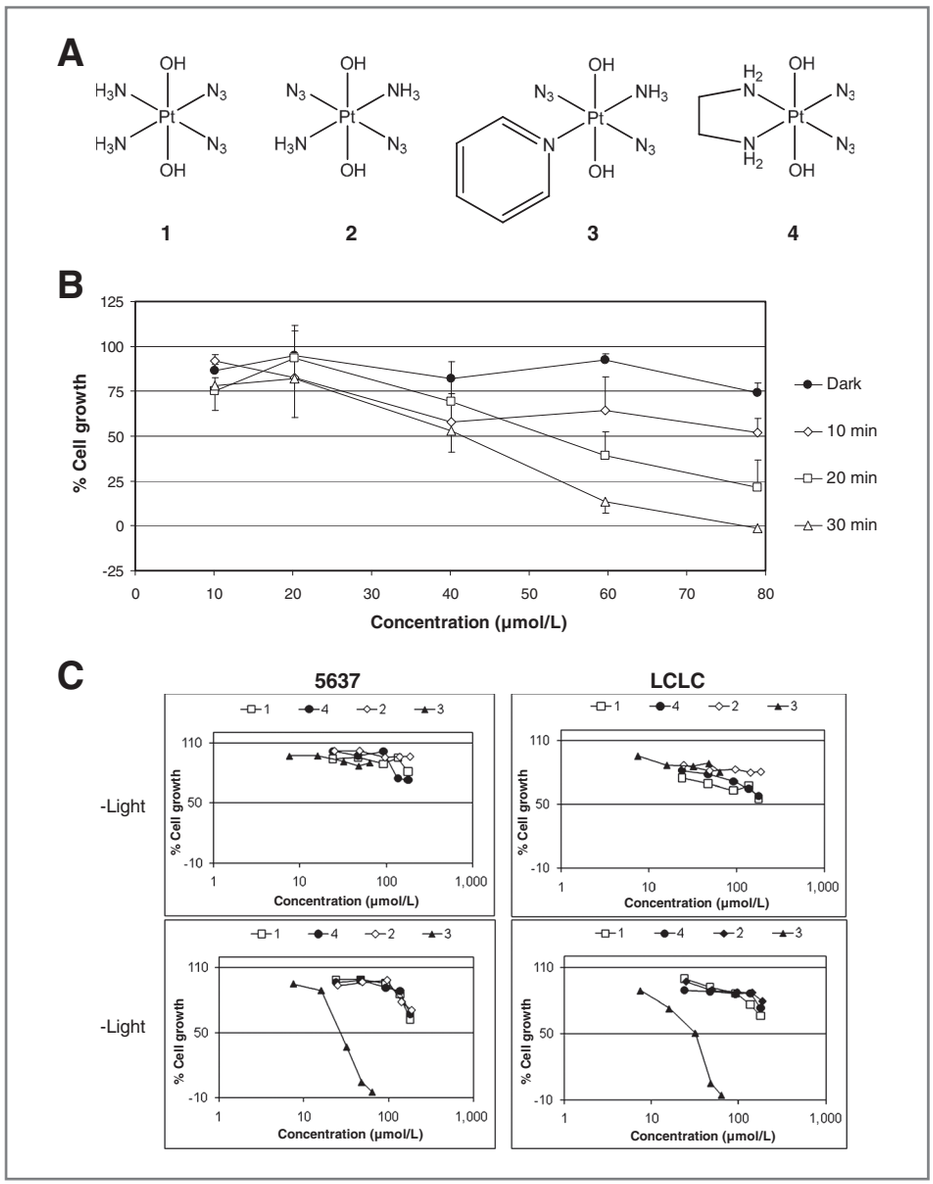

Figure 1. A, structures of diazido Pt^{IV} complexes; B, dependence of the antiproliferative effects of complex 3 in the 5637 human bladder cancer cell line on concentration and irradiation duration when irradiated with UVA ($\lambda_{max} = 366$ nm). Data from one representative experiment; values are averages + SD of 4 wells/concentration. C, effects of light (30-minute irradiation with UVA) on the growth of cancer cells treated with 4 diazido-Pt^{IV} complexes at 5 concentrations. Data from one representative experiment, values are averages of 8 wells/concentration.

different from those of classical platinum anticancer complexes. Surprising too was the activity of the all-*trans* isomer *trans*,*trans*,*trans*-$[Pt(N_3)_2(OH)_2(NH_3)_2]$, complex 2, which was as active as a cancer cell phototoxin as the *cis* diammine 1 (8). This led us to explore structure–activity relationships further and to the discovery of the potency of the *trans* pyridine/NH_3 complex *trans*,*trans*,*trans*-$[Pt(N_3)_2(OH)_2(py)(NH_3)]$, complex 3 (9). Indeed, in the series of cytotoxic *trans*-dihydroxido $[Pt(N_3)_2(OH)_2(NH_3)(X)]$ (X = alkyl or aryl amine) platinum (IV) diazido complexes, the *trans* diazido isomers are consistently more phototoxic than their *cis* diazido isomers (10).

Herein, we describe a range of biological and chemical experiments aimed at elucidating the mechanism of action of photoactivatable *trans*-diazido Pt^{IV} complexes, in particular complex 3. The work illustrates that photoexcited states can introduce novel effects on biologic pathways, which are not available to metallodrugs that act by ground state mechanisms alone.

Materials and Methods

Materials

Etoposide, E64d and pepstatin A, and fetal calf serum were from Sigma-Aldrich. RPMI-1640 culture medium was from either Sigma-Aldrich or PAN-Biotech. The Annexin V–fluorescein isothiocyanate (FITC) Kit was from Miltenyi Biotec. The LC3B and SQSTM1/p62 polyclonal antibodies were from Cell Signaling Technologies, whereas β-actin and horseradish peroxidase secondary antibodies were from Acris. Cisplatin was from Chempur.

Compounds 2 and 4 were synthesized as previously described (7–9), and compound 3 and the ^{15}N-NH_3 derivatives were prepared as described (9).

Caution! Platinum azide compounds can be explosive and should be handled with care.

Cell lines

Human cancer cell lines OE19, A2780, A2780CIS, HepG2, and SHSY5Y were obtained from the European Collection of Animal Cell Cultures (ECACC), whereas 5637, SISO, Kyse 70, Kyse 510, Kyse 510, LCLC-103H, MCF-7, YAPC, RT-4, RT-112, A-427, DAN-G, and HL60 were from the German Collection of Microorganisms and Cell Cultures (DSMZ). HaCaT keratinocytes were gifted to the Photobiology Unit, Dundee by Professor N. Fusenig (German Cancer Research Center, Heidelberg, FRG). Cells were cultured in RPMI-1640 (DSMZ and A2780 lines) or Dulbecco's Modified Eagle's Medium (ECACC lines) containing 10% fetal calf serum and passaged weekly for no longer than 6 months after resuscitation. Cell lines were free of *Mycoplasma* as determined with the Hoechst staining method and authenticated at either the DSMZ or ECACC (not by authors).

Crystal violet assay

Cells were preincubated with complexes 2, 3, and 4 for 1 hour, followed by irradiation with fluorescent white light (intensity = 0.65 mW/cm^2) or UVA (λ_{max} = 366 nm, intensity = 0.12 mW/cm^2) for up to 30 minutes. Luzchem Expo panels (Luzchem Reasearch Inc.) were used for irradiation. Lower wavelength UV radiation was blocked by a filter for both lamps. Cells were incubated for an additional 6 hours in the dark and medium was replaced. Ninety hours later medium was discarded and cells were fixed with glutaraldehyde. Staining of cells with Crystal Violet and quantification of the optical density of the cell-bound dye were done as described (11).

MTT assay

HL60 cells were seeded into 96-well microtiter plates at 10,000 cells per well, and dilutions of the compounds in cell culture medium were added to the cultures. Following 1-hour pretreatment, cultures were irradiated with light for 30 minutes, followed by 6 hours in the dark. Afterwards, the cells were centrifuged and the pellet resuspended in fresh medium. The cells grew an additional 42 hours before the MTT assay was done as described (11).

Neutral red phototoxicity assay

Cells were seeded into 96-well plates at 6×10^4 to 7×10^4 cells/cm^2. Test compounds were dissolved in Earle's Balanced Salt Solution. Chlorpromazine and photofrin were used as positive controls for UVA and visible light irradiation, respectively. Cells were treated for 1 hour and then irradiated with 5 J/cm^2 UVA or visible radiation. Cell viability was measured 24 hours later by Neutral Red dye uptake. The IC_{50} value was defined as the concentration required to inhibit dye uptake by 50%. Goodness-of-fit was determined from the r^2 values of the curves and 95% confidence intervals (CI; refs. 12, 13).

Cell-cycle studies

HL60 cells at 100,000 cells/mL were treated at the IC_{90} value of etoposide (0.74 μmol/L), cisplatin (0.74 μmol/L), or **3** (68 μmol/L). Untreated controls and cells treated with etoposide and cisplatin were incubated in the dark for 48 hours. Cells exposed to complex 3 were preincubated in the dark for 1 hour followed by a 30-minute irradiation with UV light. After 6 hours cells were centrifuged and resuspended in fresh medium. Cells treated with complex 3 were incubated in the dark for another 42 hours. One million cells from each sample were centrifuged, the supernatant discarded, and cells washed twice with PBS. The cells were resuspended in ice-cold ethanol 70% (v/v) and stored at −20°C before further analysis. After centrifugation, supernatant was removed and cells resuspended in PBS containing 25 μg/mL propidium iodide (PI) and 100 μg/mL RNase. Samples were analyzed by flow cytometry (Becton Dickinson FACSCalibur with the ModFitLT V3.0 software).

Annexin V/PI assay for apoptosis

Apoptosis in HL60 cells was determined by flow cytometry with an Annexin V–FITC Kit. Cells were treated at the IC_{50} and IC_{90} concentrations of UVA-activated complex 3 (35 and 63 μmol/L, respectively), etoposide (0.42 and 0.74 μmol/L, respectively), and cisplatin (0.42 and 0.74 μmol/L, respectively) for 24 and 48 hours, as described above, for the morphology experiments. Untreated cells were incubated 24 and 48 hours in the dark. Cell distribution was analyzed by flow cytometry (MacsQuant; Miltenyi Biotec).

Detection of LC3B and p62

HL60 cells preincubated with 100 μmol/L complex 3 in the dark for 1 hour followed by a 30-minute irradiation with UVA. After 6 hours, the cells were centrifuged and lysed in 50 mmol/L Tris (pH 7.5), 100 mmol/L NaCl, 100 mmol/L NaF, 5 mmol/L EDTA, 0.2 mmol/L Na_3VO_4, and 0.1% Triton X-100 supplemented with a protease inhibitor. Following a 5-minute sonification, the lysates were centrifugated at 18,000 × *g* for 20 minutes. Supernatant protein concentrations were determined by Bradford. Twenty micrograms of protein per lane were run on a denaturing 12% SDS-polyacrylamide gel and transferred to polyvinylidene fluoride membranes. After blocking the membrane, it was incubated overnight with various primary antibodies. After incubation with a peroxidase-conjugated secondary antibody for 1 hour, the band intensities were visualized by measuring chemiluminescence with an Intas ChemoCam (Intas Science Imaging Instruments) instrument.

Clonogenic assay

Preincubation of complex 3 with SISO cells for 1 hour was followed by irradiation for 30 minutes with UVA.

Medium was removed after 6 hours and cells washed twice with PBS before reseeding into 6-well plates. Colonies were grown in an incubator for 10 days, then stained with methylene blue and counted manually as clusters of 50 cells or more. Plating efficiency, surviving fraction, and IC_{50} values were calculated as previously described (14).

Antitumor activity in nude mice

Xenograft studies with OE19 tumors were done under Home Office license in accordance with current standards (15). Female nude mice (nu/nu) were injected subcutaneously into the flank with 1×10^8 OE19 human esophageal carcinoma cells in a 50% Matrigel suspension (total 100 μL). The mice were housed under aseptic conditions in individually ventilated cages in a temperature (24°C) and light controlled (12 hour/12 hour) environment. Animals had free access to food and water.

Compound 3 was freshly prepared in sterile water at a concentration of 1,200 μg/100 μL and sterile filtered. The drug was administered intraperitoneally in a single injection 2 hours before irradiation. Mice were irradiated under anesthesia while kept on a warming plate to maintain body temperature. Light of wavelength 420 ± 27 nm was delivered via a light guide connected to a monochromator. The equipment consisted of a 450 W xenon lamp connected to a precision-controlled monochromator fitted with order-sorting filters. Light is transmitted through a liquid light guide and output was measured, adhering to British Standards ISO9001, by using a calibrated photodiode and integrating sphere. The end of the light guide was placed on the tumor and a dose of approximately 100 J/cm^2 delivered. A second 100 J/cm^2 dose was delivered 6 hours later. The mean output at $\lambda = 420$ nm was 60 mW/cm^2.

Tumor dimensions and mouse weights were measured at least twice per week. Tumor volumes were determined by caliper measurement and were calculated using the formula $V = 4/3\pi\,[(d1 + d2)/4]^3$ mm^3. To use all the data a log-rank test was done, comparing the curves of time until a tumor size of 430 to 540 mm^3 was reached (Graphpad Prism, version 5). Relative tumor volumes were compared by using Student t test. Animals were divided into the following groups: (a) no treatment control ($n = 7$); (b) vehicle + $\lambda = 420$ nm radiation ($n = 6$); (c) complex 3 only ($n = 5$); (d) complex 3 + $\lambda = 420$ nm radiation ($n = 7$).

Nuclear magnetic resonance spectroscopy

^{14}N nuclear magnetic resonance (NMR) spectra were recorded with a Bruker DRX-500 instrument as described previously (16) or reported in the Supplementary Data section.

Computational details

Calculations were carried out with the Gaussian 03 (G03) program (17) using the density functional theory (DFT) method, the B3LYP (18), and the PBE1PBE (19) functionals. The LanL2DZ basis set (20) and effective core potential were used for the Pt atom, and the 6-31G** basis set (21) was used for all other atoms. Geometry optimizations of *trans*,*trans*,*trans*-$[Pt(N_3)_2(OH)_2(NH_3)(py)]$ in the ground state (S_0) and lowest-lying triplet state (T_1) were carried out in the gas phase, and the nature of all stationary points was confirmed by normal mode analysis. For the T_1 geometries, the UKS method with the unrestricted B3LYP or PBE1PBE functional was used. The conductor-like polarizable continuum model method (22) with water as solvent was used to calculate the electronic structure and the excited states of complex 3 in solution. Thirty-two singlet and 8 triplet excited states with the corresponding oscillator strengths were determined with a time-dependent density functional theory (TDDFT; ref. 23) calculation. The electronic distribution and the localization of the singlet excited states were visualized with the electron density difference maps (EDDM; ref. 24) GaussSum 1.05 (25) used for EDDMs calculations and for the electronic spectrum simulation. Mulliken and NBO charges of the ground-state and lowest-lying geometry were calculated with unrestricted PBE1PBE. The performances of the B3LYP and PBE1PBE functionals are consistent with results previously reported in the literature (26).

Results

Influence of light on the *in vitro* cytotoxicities of Pt^{IV} diazides

In the dark, complex 3 showed no cytotoxicity toward 5637 cells (Fig. 1B). With increasing irradiation time, 3 showed increasing antiproliferative potency (Fig. 1B). An irradiation of 30 minutes was found optimal.

We compared the phototoxicity of the *trans*-diazido complex 3 with the *cis*-diazido Pt^{IV} complex 1 and *trans*-diazido complexes 2 and *cis*,*trans*-$[Pt(en)(N_3)_2(OH)_2]$ (complex 4). The influence of a 30-minute irradiation with UVA on the potency in the 5637 and LCLC-103H lines was investigated in parallel incubations. Representative results are shown in Fig. 1C. Without irradiation, all 4 complexes had little activity, whereas UVA induced phototoxicity for all 4 compounds. However, complex 3 is noticeably more active than the other 3 compounds (Fig. 1C); thus we directed further studies at this compound.

The selectivity of complex 3 for various tumor types was determined in 13 cancer cell lines under identical conditions by comparing IC_{50} values (Table 1). Values ranged from 29 μmol/L for RT-112 line to 137 μmol/L for RT-4 with the average IC_{50} 55 ± 28 μmol/L. In an additional 5 cell lines not resistant to cisplatin, the IC_{50} values, determined by the Neutral Red assay, ranged between 1.9 and 10 μM. (Table 2).

Light activation of complex 3 can take place outside of cells. When complex **3** was irradiated with UVA in culture medium for 30 minutes under the same conditions described above and then added to cultures of either 5637 or RT-4 cells for 6 hours followed by a 90-hour incubation in fresh medium, no significant changes in the IC_{50} values (53.5 ± 15.2 and 72.6 ± 7.5 μmol/L for 5637 and RT-4, respectively) were observed compared with those reported in Table 1.

The ability of fluorescent white and blue visible light to activate complex 3 was investigated in some of the cell

Table 1. IC_{50} values for complex 3 in various human cancer cell lines when irradiated with UV light λ_{max} = 366 nm (0.216 J/cm^2) or white light (in parentheses; 1.17 J/cm^2) for 30 minutes at 37°C

Cell line	IC_{50} value (μmol/L) ± SD	Cell line	IC_{50} value (μmol/L) ± SD	Cell line	IC_{50} value (μmol/L) ± SD
5637	30.7 ± 5.0 (69.27 ± 7.2)[a]	Kyse 510	52.9 ± 4.0	RT-4	136.9 ± 55.0
5637-OXO[b]	33.0 ± 8.51 [1.08][c]	Kyse 520	66.2 ± 8.7	RT-112	28.6 ± 3.0
SISO	43.4 ± 23.7 (59.15 ± 4.52)[a]	LCLC-103 H	38.8 ± 14.2	A-427	40.6 ± 8.3 (61.8 ± 31.62)[a]
SISO-OXO[b]	38.1 ± 15.7 [0.88][c]	MCF-7	62.0 ± 13.2	DAN-G	68.2 ± 22.6 (60.78 ± 31.6)[a]
Kyse 70	50.5 ± 4.5	YAPC	57.9 ± 17.7	HL60	35.1 ± 8.4
Kyse 70-OXO[b]	60.6 ± 4.1 [1.20][c]				

NOTE: Values are averages ± SD of 3 or more independent determinations. Cell proliferation determined by the crystal violet assay, except the HL60 line, in which the MTT assay was used.

[a]IC_{50} values determined for white light.

[b]Resistance factors for cisplatin and oxoplatin with 5637-OXO were 2.89 and 3.42, respectively; with SISO-OXO 2.07 and 3.07, respectively; with KYSE-70-OXO 2.38 and 2.09, respectively.

[c]Resistance factor = $IC_{50\ resistant}/IC_{50\ wild}$.

lines. Table 1 shows that IC_{50} values for the 5637, SISO, A-427, and DAN-G lines are approximately 2-fold greater (values in parentheses) when white light was used as compared with UVA. In OE19 cancer cells and HaCaT skin keratinocytes (Table 2), the complex was approximately 3-fold more effective in the presence of blue light, compared with the sham-irradiated controls. Thus, deeper-penetrating visible light can also activate complex 3, although not as efficiently as UVA radiation. These data are consistent with the density functional calculations that optical transitions exist for complex 3 in the visible region of the spectrum.

Investigations with cisplatin and oxoplatin-resistant cancer cell lines

Oxoplatin (*cis*,*trans*,*cis*-[$PtCl_2(OH)_2(NH_3)_2$]) undergoes chemical reduction to cisplatin and is believed to be a prodrug for cisplatin *in vivo* (27). Three cell lines 5637, SISO, and KYSE-70 made 2- to 3.4-fold resistant to oxoplatin (i.e., 5637-OXO, SISO-OXO, and KYSE-70-OXO) are also cross-resistant to cisplatin (Table 1). Consistent with the hypothesis that complex 3 acts via a mechanism distinct from cisplatin is the observation that complex 3 shows no cross resistance to these resistant cell lines, as evidenced by resistant factors close to 1 (values in brackets in Table 1). On the other hand, a fourth cell line, A2780CIS, which was made approximately 5-fold resistant to cisplatin compared with the parent line A2780, showed even stronger (9-fold) cross-resistance to UVA-activated complex 3 (Table 2) when cytotoxicity was assessed by Neural Red uptake.

Effects on the morphology and cell-cycle distribution of HL60 cells treated with cisplatin and etoposide compared with UVA-activated complex 3

Figure 2A shows the changes in cell morphology when HL60 cells are treated either with cisplatin, etoposide, or UVA-activated complex 3. When cells were exposed to

Table 2. IC_{50} values after irradiation of **3** with 5 J/cm^2 UVA radiation (λ_{max} = 365 nm; cut-off below 320 nm)

	IC_{50} value (μmol/L; 95% CI)		
Cell type	5 J/cm^2 UVA	Sham	5 J/cm^2 TL03
HaCaT	6.8 (5.4–8.6)	>244.4	86.0 (43.7–169.0)
HepG2	5.0 (3.7–6.7)	>244.4	NT[b]
A2780	1.9 (1.8–2.1)	>244.4	NT
A2780CIS[a]	16.9 (14.2–20.3)	>244.4	NT
SHSY5Y	2.0 (1.5–2.7)	>244.4	NT
OE19	10.0 (8.3–12.1)	>244.4	32.0 (13.3–76.8)

NOTE: HaCaT and OE19 cells were also irradiated with 5 J/cm^2 blue visible light, TL03 (λ_{max} = 420 nm; cut-off below 400 nm) in a separate set of experiments at 37°C. Cell proliferation determined by the Neutral Red phototoxicity assay. Data represent the mean of 6–9 monolayers from 2–3 independent experiments.

[a]5-fold resistance to cisplatin.

[b]NT: Not tested.

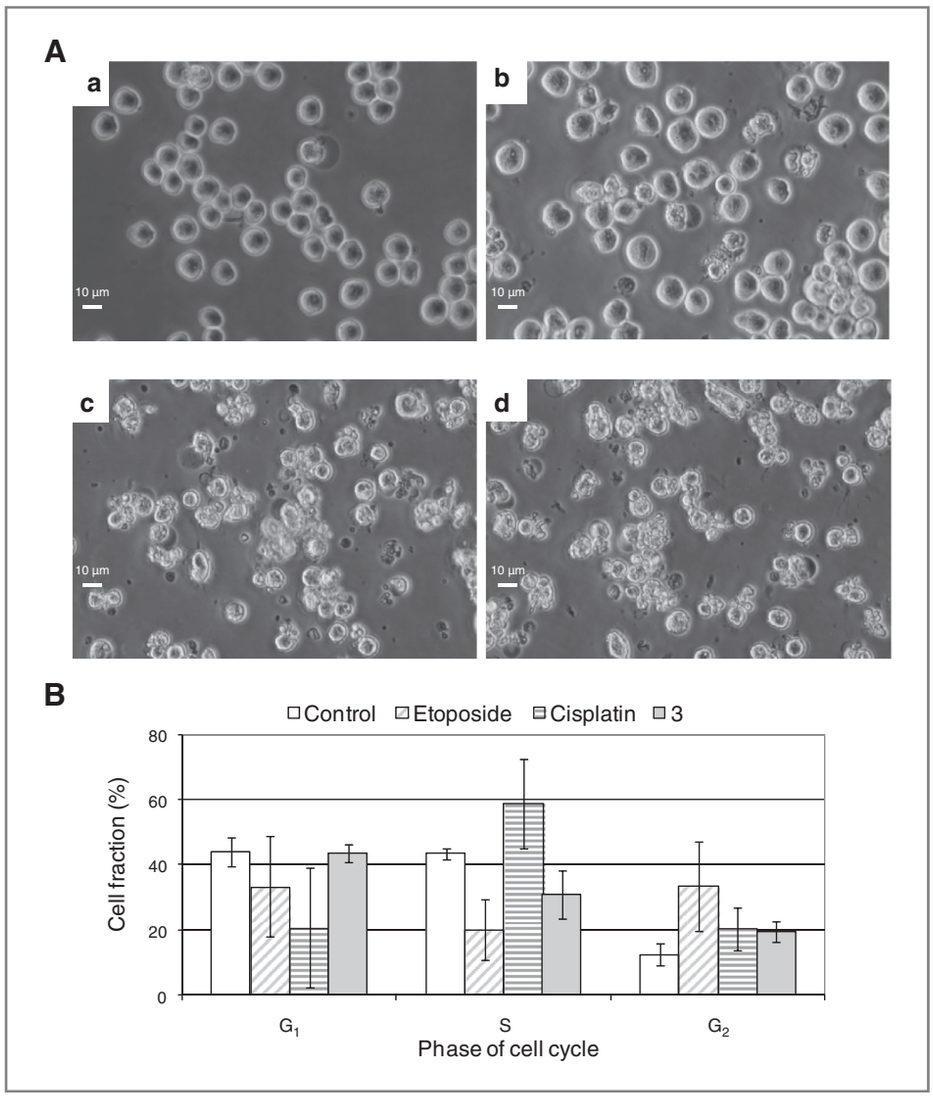

Figure 2. A, phase contrast photos (magnification, ×400) showing morphologic changes in HL60 cells treated for 48 hours with untreated control (a); 68 μmol/L complex 3 (UVA activated; b); 0.74 μmol/L cisplatin (c); 0.74 μmol/L etoposide representing the IC_{90} values (d). B, cell-cycle analysis of HL60 cells after exposure to 0.74 μmol/L etoposide, 0.74 μmol/L cisplatin, or 68 μmol/L complex 3 (UVA activated) for 48 hours compared with control, staining with PI. Results are the averages ± SD of 3 independent experiments.

etoposide or cisplatin, formation of characteristic apoptotic cells was observed; that is, cells shrink and membrane blebbing occurred (Fig. 2A, c and d; ref. 28). In contrast, cells treated with complex 3 did not show such changes but instead swelled slightly (Fig. 2A, b).

Figure 2B presents the results of the cell-cycle analysis after HL60 cells were treated with an IC_{90} concentration of either etoposide, cisplatin, or complex 3 for 1 hour, then activated for 30 minutes by UVA. For etoposide, a noticeable decrease of cells in the S phase is seen whereas cells in the G_2 phase increase by a comparable amount. This is consistent with a G_2–M arrest of the cells, as has been reported for etoposide (29). For cells treated with cisplatin, a decrease in the fraction of cells in the G_1 phase with an increase in the fraction of cells in the S and G_2 phases is consistent with a S–G_2 arrest, as has been reported previously for cisplatin in the L1210 and CHO cell lines (30). Conversely, complex 3 brought little change in the cell phase distribution: G_1 was unchanged, S was slightly decreased, and the G_2 cell fraction was somewhat increased. Thus, complex 3 does not have specific effects on the cell cycle.

Apoptosis in cells treated with cisplatin and etoposide compared with UVA-activated complex 3

Supplementary Fig. S1 shows representative results of flow cytometric examinations of nontreated HL60 cells, double-stained with Annexin V–FITC/PI, compared with those obtained with cells treated for 24 and 48 hours at the IC_{90} concentrations of cisplatin, etoposide, and UVA-activated complex 3. Figure 3A summarizes these results for 48-hour time point. Both cisplatin and etoposide strongly induced apoptosis (15%–20% of the cells). On the other hand, UVA-activated complex 3 caused only a small fraction (5% or less) of the cells to enter apoptosis; only at the IC_{90} concentration was this small increase statistically

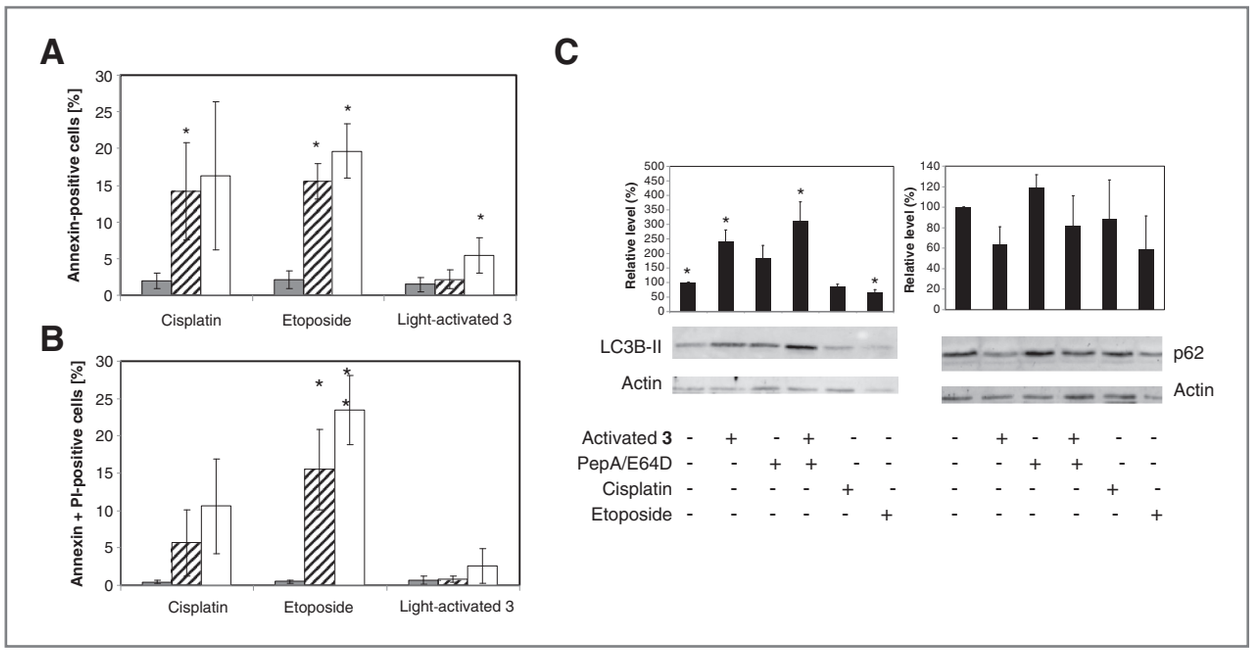

Figure 3. A, flow cytometric distribution of HL60 cells 48 hours after treatment with either cisplatin, etoposide, or light-activated complex 3 at either the IC_{50} (slashed bars) or IC_{90} (open bars) concentrations. Gray bars, untreated controls. Apoptotic fraction of cells that were stained only with Annexin V–FITC. B, dead/necrotic fraction of cells that were stained with both Annexin V–FITC and PI. Values represent the averages of 4 independent experiments and error bars are SDs. C, levels of LC3B-II and p62 in HL60 cells 6 hours after treatment with either UVA activated complex 3 (100 μmol/L), cisplatin (0.74 μmol/L), or etoposide (0.74 μmol/L) in the presence or absence of the lysosomal protease inhibitors pepstatin A (10 μg/mL) and E64D (10 μg/mL). Cells were preexposed to complex 3 in the dark for 1 hour followed by a 30-minute irradiation with UV light. Total protein extracts were analyzed for LC3B-II and p62 by using Western blot analysis to detect autophagic flux. Representative immunoblots are shown. Graphs show average results of 3 independent determinations with SD. * significantly different to untreated controls tested by paired, 2-tailed *t* test, $P < 0.05$.

significant. In Fig. 3B the fraction of dead/necrotic cells that stained positive with both Annexin V–FITC and PI are shown. Here again, both cisplatin and etoposide at both the IC_{50} and IC_{90} concentrations were effective at inducing apoptotic cell death, although treatment with UVA-activated complex 3 caused little apoptosis.

Microscopic analysis of Hoechst 33342-stained nuclei from A2780 cells treated with either cisplatin or UVA-activated complex 3 support the idea that cells do not die by apoptosis. Supplementary Fig. S2 shows that although treatment of A2780 cells with cisplatin resulted in a time-dependent increase in condensed and fragmented nuclei typical of caspase-dependent apoptosis; treatment with complex 3 did not.

Activation of autophagic pathways by UVA-activated complex 3

The possibility that autophagy is involved in cell death was investigated by monitoring the cellular levels of 2 key proteins; microtubule-associated protein light chain 3 (LC3), a ubiquitin-like protein associated with autophagosome, and sequestosome 1 (p62), a protein that becomes incorporated into the autophagosome and is degraded by the autolysome during autophagy (31, 32). Western blots in Fig. 3C show a 2.5-fold increase in the levels of LC3B-II in HL60 cells treated with 100 μmol/L UVA-activated complex 3 for 6 hours compared with controls. (LC3B-I was not visible in our blots). The lysosomal protease inhibitors E64d and pepstatin A increased the levels of LC3B-II still further, consistent with a blockage of LC3B-II degradation (31). Cisplatin and etoposide caused no increases in LC3B-II levels, probably because they induce apoptosis. The cellular levels of p62 consistently dropped on the average by 40% in cells treated with UVA-activated complex 3, but these changes were not significant. Thus, autophagic pathways seemed to be activated by UVA-activated complex 3 (31).

Clonogenic assay in the human cervix adenocarcinoma cancer cell line SISO

The clonogenic assay is more appropriate than measuring antiproliferative activty *in vitro* for predicting antitumor activity (14, 33). With the SISO cell line, complex 3 was approximately 10-fold more potent in the clonogenic assay compared with the crystal violet assay (IC_{50} values of 4.94 ± 2.76 and 43.4 ± 23.7 μmol/L, respectively). Cisplatin had an anticlonogenic IC_{50} value of 0.20 ± 0.02 μmol/L. Although, complex 3 is 25-fold less potent in this assay compared with cisplatin, it clearly shows antitumor potential.

Antitumor activity of complex 3 in mice bearing xenografted OE19 tumors

The results of the clonogenic assay encouraged us to investigate the antitumor activity of complex 3 with and

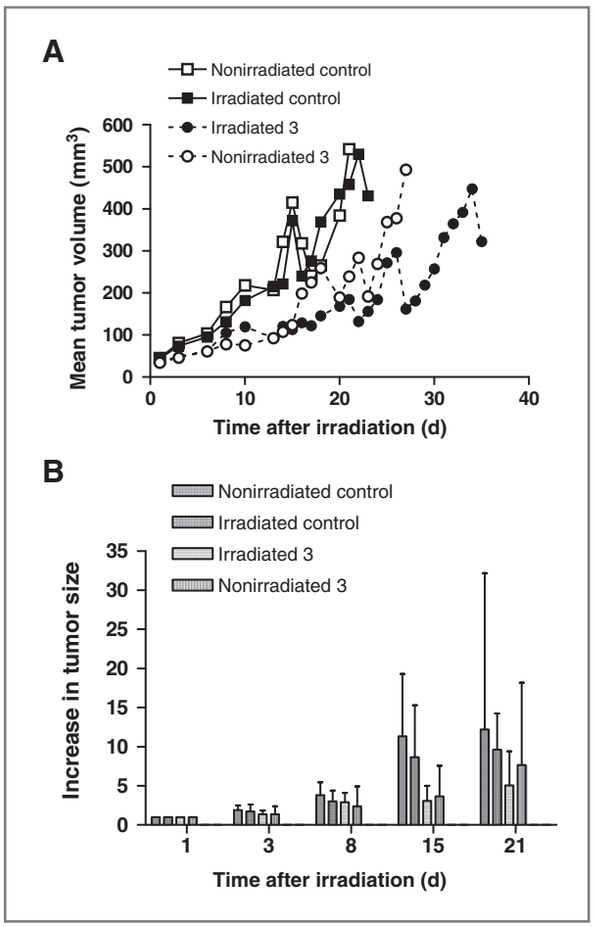

Figure 4. Antitumor studies in female nude mice bearing xenograph OE19 tumors. A, mean tumor volume plotted against time after irradiation. B, tumor volumes (means ± 95% CI) normalized to day 1 (day of injection and irradiation).

without irradiation in nude mice bearing xeongraft OE19 tumors. Tumor volumes were determined at least twice weekly. Figure 4 shows that complex 3 has antitumor activity *in vivo*, which is photoaugmented with visible light. At day 21, 3 of 7 nonirradiated control mice survived; 4 of 6 irradiated control mice survived; 4 of 5 nonirradiated complex 3 mice survived, and 7 of 7 irradiated complex 3 mice survived (i.e., the tumors had not reached the size requiring euthanasia). At day 35 when the experiment was ended, none of 7 nonirradiated control mice survived; none of 6 irradiated control mice survived; none of 5 nonirradiated complex 3 mice survived; and 2 of 7 irradiated complex 3 mice survived. A log-rank test was done comparing the curves of time until tumor size reached 430 to 540 mm^3 and found no difference between the nonirradiated versus irradiated controls. There was a difference between controls and irradiated complex 3 ($P = 0.0029$; HR, 9.6; 95% CI, 2.2–42.2). The P value for controls versus nonirradiated complex 3 was $P = 0.055$ (HR, 3.7; 95% CI, 1.0–13.8). The P value between irradiated complex 3 and nonirradiated complex 3 was $P = 0.055$. In Fig. 4B the tumor volumes at the indicated time points are expressed relative to the initiating volume. Despite the administered dose of complex 3 being in the region of 10 times the maximum tolerated dose of cisplatin, mice remained alert and active, with no behavioral changes or signs of morbidity. There was no evidence of oculocutaneous phototoxicity (Fig. 4A and B).

Photochemistry

Irradiation of **3** with UVA radiation ($\lambda_{max} = 351$ nm) was monitored by ^{14}N NMR spectroscopy in physiologic buffer A solution. Assignment of the ^{14}N NMR resonances was aided by comparison of the $^{15}NH_3$-labeled and unlabeled complexes (Supplementary Fig. S3). $^{14}N\{^1H\}$ NMR spectra of complex 3 (20 mmol/L in PBA) acquired after irradiation for 0, 30 minutes (10 J/cm^2), and 2 hours (41 J/cm^2) with UVA show the release of free azide following irradiation (Supplementary Fig. S4), as is observed for *cis,trans,cis*-$[Pt^{IV}(N_3)_2(OH)_2(NH_3)_2]$ (34) and the all-*trans* isomer under similar conditions (35).

No free pyridine was detected either by ^1H or ^{14}N NMR spectroscopy. This suggests that pyridine might play a role in any subsequent recognition (or nonrecognition) of platinated lesions, for example, on DNA, as has been found to be the case for DNA GN7 adduct of *cis*-$\{Pt(NH_3)_2(pyridine)\}^{2+}$, in which the bulky pyridine sterically blocks translocation by RNA polymerase (36).

Calculations of electronic states

DFT and TDDFT were used to characterize singlet and triplet excited states for complex 3. Such computational methods can be used successfully to obtain insights into the photophysical (refs. 37–39; e.g., absorption) and photochemical (40, 41) properties of metal complexes.

The theoretical UV-Vis spectrum (Supplementary Fig. S5) simulated by TDDFT shows that the band in the UV region is composed of transitions with a prevalent ^{1}LMCT character (see Supplementary Data). Interestingly, TDDFT also shows that weak transitions (Supplementary Fig. S5 inset, transitions S1–S3) are present in the UVA and visible regions of the spectrum. These have ^{1}LMCT character and are of dissociative nature because of the significant contributions from the σ-antibonding LUMO and LUMO+2 orbitals (Supplementary Fig. S6A and B). Particularly for the LUMO, the strong antibonding character is toward the Pt–N_3 bonds. This is consistent with the activation of complex 3 by visible light and with the observed light-induced release of N_3 ligands.

Strong spin-orbit coupling of the Pt atom can promote efficient intersystem crossing and formation of triplet states, which are likely to play a role in the photoreactivity of complex 3. All calculated triplets have dissociative nature confirming the high photoreactivity of complex 3. Furthermore, optimization of the lowest-lying triplet state geometry provided a distorted triplet-state structure, in which one azide ligand is displaced (Pt–N_3 = 3.590 Å) and the second has a Pt–N_3 distance elongated by 0.235 Å compared with the ground state

(Supplementary Fig. S6B). Therefore, upon intersystem crossing and population of the lowest-lying triplet, the dissociation of one or both azide ligands can occur. Analysis of atomic charges and electronic configuration showed that in the lowest-lying triplet geometry, both azides are less negatively charged, whereas the Pt center is less positively charged. Such behavior can account for a $Pt^{IV} \rightarrow Pt^{II}$ reduction mechanism and for the formation of $N_3^{\bullet}$ A radical fragments.

Discussion

There is growing interest in developing photoactivatable cytotoxic agents for cancer treatment. Photoactivated chemotherapy would be expected to have a higher therapeutic index compared with traditional chemotherapy. Owing to their rich photochemistry, transition metal complexes in general and platinum agents in particular are strong candidates for this purpose (3, 42–44). Pt^{IV} diazides have interesting photobiologic properties in cellular systems (7–10), and the aim of this work was to elucidate the complex mechanism of action of one potent compound in this class (i.e., complex 3). Although these complexes were initially designed as light-activatable Pt prodrugs of cytotoxic Pt^{II} diamines (e.g., cisplatin), the results reported here indicate that other novel mechanisms of cytotoxicity are involved.

The experiments with various cancer cell lines provide new evidence that cytotoxicity induced by light activation of complex 3 is distinct from that observed with cisplatin: First, we show here for the first time that complex 3 has little selectivity toward the 13 cancer cell lines studied, in contrast to cisplatin, which is selective for the SISO, KYSE-70, DAN-G, and 5637 cell lines (11). Second, no cross-resistance was observed with 3 oxoplatin-resistant cell lines, which are all completely cross-resistant to cisplatin. Third, the morphologies of HL60 cells following exposure to equicytotoxic doses are very different from cells treated with either cisplatin or etoposide, 2 drugs that activate caspase-3 and induce apoptosis in this cell line. Moreover, cell distribution among the phases of the cell cycle following exposure to these 3 agents at their IC_{90} values is different; whereas cisplatin and etoposide cause $S–G_2$ and $G_2–M$ arrests, respectively, complex 3 has only a weak influence on the overall distribution. Here we report that UVA-activated complex 3, unlike cisplatin and etoposide, is ineffective in causing the redistribution of phosphotidylserine of HL60 cells from the cytosolic surface of the plasma membrane to the outer layer of the bilayer, a hallmark of early apoptosis. Thus, apoptosis is unlikely to be an important mechanism of cell death, in agreement with our previous finding that UVA-activated complex 3 does not activate caspase-3 (9).

Autophagic cell death may be more important in cancer chemotherapy than once appreciated (45). A number of autophagic pathways, including LC3 and p62, can be monitored to help establish autophagy in the death of cells caused by a cytotoxic drug (32, 33). For example, glioma cells treated with temozolomide increased both transcription of the LC3 gene and LC3 aggregation during autophagic death (46). Hepatocellular carcinoma cell lines treated with a cytotoxic COX-2 inhibitor, OSU-03012, showed a dose-dependent increased in levels of the LC3-II protein (47). It was shown that pediatric brain tumor cell lines exposed for 8 hours at the IC_{50} doses of either rapamycin, lomustin, or cisplatin caused an increase in the levels of LC3 and a decrease in the levels of p62 (48). In our work, we detected a significant increase in levels of LC3B-II when HL60 cells were exposed for 6 hours to UVA-activated complex 3, consistent with autophagy. Also consistent with an autophagic mechanism was the reproducible decrease in levels of p62 in the treated cells relative to controls, but this change was not significant. Thus, in the absence of apoptosis, autophagy becomes activated during cell death.

Another important finding was that complex 3 can be activated not only with UVA but also with visible light. Although visible light was somewhat less effective in activating the complex, this is important when considering the therapeutic potential of such a drug; that is, deeper penetration of visible light into tumor tissue compared with UVA is necessary for successful application of the complex in cancer treatment.

The data from clonogenic assays are supportive of an antitumor effect. Indeed, the complex showed antitumor activity against OE19 cells subcutaneously transplanted into the flanks of the animals. The antitumor activity of complex 3 was augmented by 2×100 J/cm^2 of 420-nm blue light delivered through the skin for approximately 30 minutes, 2 hours after a single injection, followed by a second irradiation 6 hours later (a cumulative dose of approximately 200 J/cm^2). This seems to be the first report of the successful use of light to enhance the anticancer activity of a metal-based drug *in vivo*. Importantly, the compound showed no apparent toxicity in mice, even when given at a dose 10-fold greater than that typically used with cisplatin. It should be noted that the animals were not kept in darkness, but on a 12/12 light cycle in partially transmitting polymer cages; therefore we cannot exclude ambient light photoaugmetation of the nonirradiated complex 3 group.

The question arises as to the nature of the cytotoxic species formed from light activation. In previous work we found that light activation of complex 3 resulted in an accumulation of Pt in 5637 cells more rapidly than when the complex was not photolyzed (49). This suggests that photolysis yields reactive Pt species that irreversibly bind to cellular components. Consistent with this, we have found that upon irradiation with UVA and white light, complex 3 is reduced to the Pt(II) complex $[Pt(OH)_2NH_3(pyridine]$ as well as Pt species that irreversibly platinate calf thymus DNA (50). Thus, DNA could be one target for photoactivated complex 3 but, unlike when cisplatin binds to DNA, initiates little apoptosis. Although Pt^{II} species may be involved in the cytotoxicity, other reactive species unique to this complex could also be

important. Our NMR studies show that NH_3, N_2, and azide are released from complex 3 on photochemical activation. Thus, reactive species other than Pt-based may be involved in cytotoxicity. Nevertheless, our data indicate that photolysis products can form outside of cells and still be effective cytotoxic agents.

TDDFT calculations confirmed the dissociative character of excited states and revealed the presence of weak transitions in the visible region of the spectrum. Photochemical reactions of Pt^{IV} azides are known to generate Pt^{IV} nitrenes and azido radicals in addition to Pt^{II} species (4). Such a combination of species generated in cells may rapidly affect a variety of biochemical pathways. On the basis of their extreme chemical reactivity, Pt^{IV}-nitrenes and azido radicals would be expected to be toxic to cells by a mechanism independent of DNA binding.

In conclusion, these studies provide new insights in the photoinduced cytotoxic mechanism of *trans*-diazido Pt^{IV} complexes. Moreover, light-activated complex 3 has antitumor activity *in vivo*. The mechanism of cytotoxicity *in vitro* is different from that of cisplatin, and autophagy is implicated. These results show that excited states of metal-based anticancer drugs can introduce novel mechanisms of action, which may be valuable in clinical use.

Disclosure of Potential Conflicts of Interest

P.J. Sadler has ownership interest (including patents) by patent application GB0120618.

Acknowledgments

The authors thank Kerstin Gumm, Anne Schüttler, and Gudrum Schüster for technical assistance, Dr. Luca Ronconi and members of COST Action D39 for fruitful discussions.

Grant Support

This work was supported by Marie Curie Intra European Fellowship 220281 (L. Salassa), and grants EP/G006792/1 from the Engineering Physical Science Research Council (P.J. Sadler), G0701062 from Medical Research Council (P.J. Sadler and J.A. Woods), 247450 from European Research Council (P.J. Sadler), 230805876 from Breast Cancer Research, Scotland (V. Appleyard and K. Murry) and SY/SP8012 from Science City/Advantage West Midlands & European Regional Development Fund (P.J. Sadler).

The costs of publication of this article were defrayed in part by the payment of page charges. This article must therefore be hereby marked *advertisement* in accordance with 18 U.S.C. Section 1734 solely to indicate this fact.

Received November 23, 2011; revised May 14, 2012; accepted May 15, 2012; published OnlineFirst June 18, 2012.

References

1. Ronconi L, Sadler PJ. Applications of heteronuclear NMR spectroscopy in biological and medicinal inorganic chemistry. Coord Chem Rev 2007;251:1633–48.
2. Kratochwil NA, Zabel M, Range KJ, Bednarski PJ. Synthesis and X-ray crystal structure of trans,cis-[$Pt(OAc)_2I_2(en)$]: A novel type of cisplatin analog that can be photolyzed by visible light to DNA-binding and cytotoxic species *in vitro*. J Med Chem 1996;39:2499–507.
3. Bednarski PJ, Mackay FS, Sadler PJ. Photoactivatable platinum complexes. Anti-Cancer Agents Med Chem 2007;7:75–93.
4. Šima J. Photochemistry of azide-moiety containing inorganic compounds. Coord Chem Rev 2006;250:2325–34.
5. Müller P, Schroder B, Parkinson JA, Kratochwil NA, Coxall RA, Parkin A, et al. Nucleotide cross-linking induced by photoreactions of platinum(IV)-azide complexes. Angew Chem-Int E 2003;42:335–9.
6. Kasparkova J, Mackay FS, Brabec V, Sadler PJ. Formation of platinated GG cross-links on DNA by photoactivation of a platinum(IV) azide complex. J Biol Inorg Chem 2003;8:741–5.
7. Bednarski PJ, Grunert R, Zielzki M, Wellner A, Mackay FS, Sadler PJ. Light-activated destruction of cancer cell nuclei by platinum diazide complexes. Chem Biol 2006;13:61–7.
8. Mackay FS, Woods JA, Moseley H, Ferguson J, Dawson A, Parsons S, et al. A photoactivated trans-diammine platinum complex as cytotoxic as cisplatin. Chem Eur J 2006;12:3155–61.
9. Mackay FS, Woods JA, Heringova P, Kasparkova J, Pizarro AM, Moggach SA, et al. A potent cytotoxic photoactivated platinum complex. Proc Nat Acad Sci U S A 2007;104:20743–8.
10. Farrer NJ, Woods JA, Munk VP, Mackay FS, Sadler PJ. Photocytotoxic trans-diam(m)ine platinum(IV) diazido complexes more potent than their cis isomers. Chem Res Toxicol 2010;23:413–21.
11. Bracht K, Boubakari, Grünert R, Bednarski PJ. Correlations between the activities of 19 antitumor agents and the intracellular glutathione concentrations in a panel of 14 human cancer cell lines: comparisons with the National Cancer Institute data. Anti-Cancer Drugs 2006; 17:41–51.
12. Traynor NJ, Barratt MD, Lovell WW, Ferguson J, Gibbs NK. Comparison of an *in vitro* cellular phototoxicity model against controlled clinical trials of fluoroquinolone skin phototoxicity. Toxicol in Vitro 2000; 14:275–83.
13. Moseley H. Scottish UV dosimetry guidelines, "ScUViDo". Photodermatol Photoimmunol Photomed 2001;17:230–3.
14. Franken NAP, Rodermond HM, Stap J, Haveman J, van Bree C. Clonogenic assay of cells *in vitro*. Nature Prot 2006;1:2315–9.
15. Workman P, Aboagye EO, Balkwill F, Balmain A, Bruder G, Chaplin DJ, et al. Guidelines for the welfare and use of animals in cancer research. Br J Cancer 2010;102:1555–77.
16. Farrer NJ, Gierth P, Sadler PJ. Probing platinum azido complexes by ^{14}N and ^{15}N NMR spectroscopy. Chem Eur J 2011;7:12059–66.
17. Frisch MJ, Trucks GW, Schlegel HB, Scuseria GE, Robb MA, Cheeseman JR, et al. Gaussian 03, revision D 0.1; Gaussian Inc.: Wallingford CT; 2004.
18. Becke AD. Density-functional thermochemistry 3. The role of exact exchange. J Chem Phys 1993;98:5648–52.
19. Perdew JP, Burke K, Ernzerhof M. Generalized gradient approximation made simple. Phys Rev Lett 1996;77:3865–8.
20. Hay PJ, Wadt WR. *Ab-initio* effective core potentials for molecular calculations–potentials for the transition-metal atoms Sc to Hg. J Chem Phys 1985;82:270–83.
21. McLean AD, Chandler GS. Contracted Gaussian-basis sets for molecular calculations 1. 2^{nd} row atoms, $Z = 11$-18. J Chem Phys 1980; 72:5639–48.
22. Cossi M, Rega N, Scalmani G, Barone V. Energies, structures, and electronic properties of molecules in solution with the C-PCM solvation model. J Comput Chem 2003;24:669–81.
23. Casida ME, Jamorski C, Casida KC, Salahub DR. Molecular excitation energies to high-lying bound states from time-dependent density-functional response theory: Characterization and correction of the time-dependent local density approximation ionization threshold. J Chem Phys 1998;108:4439–49.
24. Browne WR, O'Boyle NM, McGarvey JJ, Vos JG. Elucidating excited state electronic structure and intercomponent interactions in multicomponent and supramolecular systems. Chem Soc Rev 2005; 34:641–63.

25. O'Boyle NM, Tenderholt AL, Langner KM. cclib: A library for package-independent computational chemistry algorithms. J Comp Chem 2008;29:839–45.
26. Jacquemin D, Perpète EA, Ciofini I, Adamo C. Accurate simulation of optical properties in dyes. Acc Chem Res 2009;42:326–34.
27. Hamberger J, Liebeke M, Kaiser M, Bracht K, Olszewski U, Zeillinger R, et al. Characterization of chemosensitivity and resistance of human cancer cell lines to platinum(II) versus platinum(IV) anticancer agents. Anticancer Drugs 2009;20:559–72.
28. Fadeel B, Orrenius S. Apoptosis: a basic biological phenomenon with wide-ranging implications in human disease. J Inter Med 2005; 258:479–517.
29. Facompre M, Wattez N, Kluza J, Lansiaux A, Bailly C. Relationship between cell cycle changes and variations of the mitochondrial membrane potential induced by etoposide. Mol Cell Biol Res Commun 2000;4:37–42.
30. Eastman A. The mechanism of action of cisplatin: From adducts to apoptosis. In:Lippert B, editor. Cisplatin. Chemistry and biochemistry of a leading anticancer drug. Weinheim: Wiley-VCH; 1999. p. 111–34.
31. Mizushim N, Yoshimori T. How to interpret LC3 immunoblotting. Autophagy 2007;3:542–5.
32. Klionsky DJ, Abeliovich H, Agostinis P, Agrawal DK, Aliev G, Askew DS, et al. Guidelines for the use and interpretation of assays for monitoringautophagy in higher eukaryotes. Autophagy 2008;4:151–75.
33. Puck TT, Marcus PI. Action of X-rays on mammalian cells. J Exper Med 1956;103:653–66.
34. Phillips HIA, Ronconi L, Sadler PJ. Photoinduced reactions of cis, trans,cis-[Pt(IV)$(N_3)_2(OH)_2(NH_3)_2$] with 1-methylimidazole. Chem Eur J 2009;15:1588–96.
35. Ronconi L, Sadler PJ. Photoreaction pathways for the anticancer complex trans,trans,trans-[Pt$(N_3)_2(OH)_2(NH_3)_2$]. Dalton Trans 2011; 40:262–8.
36. Wang D, Zhu GY, Huang XH, Lippard SJ. X-ray structure and mechanism of RNA polymerase II stalled at an antineoplastic monofunctional platinum-DNA adduct. Proc Nat Acad Sci USA 2010;107:9584–9.
37. Vlcek A, Zalis S. Modeling of charge-transfer transitions and excited states in d(6) transition metal complexes by DFT techniques. Coord Chem Rev 2007;251:258–87.
38. Salassa L, Garino C, Albertino A, Volpi G, Nervi C, Gobetto R, et al. Computational and spectroscopic studies of new rhenium(I) complexes containing pyridylimidazo[1,5-a]pyridine ligands: Charge transfer and dual emission by fine-tuning of excited states. Organometallics 2008;27:1427–35.
39. Garino C, Gobetto R, Nervi C, Salassa L, Rosenberg E, Ross JBA, et al. Spectroscopic and computational studies of a Ru(II) terpyridine complex: The importance of weak intermolecular forces to photophysical properties. Inorg Chem 2007;46:8752–62.
40. Salassa L, Garino C, Salassa G, Gobetto R, Nervi C. Mechanism of ligand photodissociation in photoactivable $[Ru(bpy)_2L_2]^{2+}$ complexes: A density functional theory study. J Am Chem Soc 2008;130:9590–7.
41. Salassa L, Garino C, Salassa G, Nervi C, Gobetto R, Lamberti C, et al. Ligand-selective photodissociation from $[Ru(bpy)(4AP)_4]^{2+}$: a spectroscopic and computational study. Inorg Chem 2009;48:1469–81.
42. Schatzschneider U. Photoactivated biological activity of transition-metal complexes. Eur J Inorg Chem 2010;10:1451–67.
43. Nagy EM, Via LD, Ronconi L, Fergona D. Recent advances in PUVA photochemotherapy and PDT for the treatment of cancer. Curr Pharm Design 2010;16:1863–76.
44. Ciesienski KL, Franz KJ. Keys for unlocking photolabile metal-containing cages. Angew Chem Int Ed 2011;50:814–24.
45. Yang ZNJ, Chee CE, Huang SB, Sinicrope FA. The role of autophagy in cancer: Therapeutic implications. Mol Cancer Ther 2011;10: 1533–41.
46. Kanzawa T, Germano IM, Komata T, Ito H, Kondo Y, Kondo S. Role of autophagy in temozolomide-induced cytotoxicity for malignant glioma cells. Cell Death Diff 2004;11:448–57.
47. Gao M, Yeh PY, Lu YS, Hsu CH, Chen KF, Lee WC, et al. OSU-03012, a novel celecoxib derivative, induces reactive oxygen species-related autophagy in hepatocellular carcinoma. Cancer Res 2008;68: 9348–57.
48. Mulcahy Levy JM, Thorburn A. Modulation of pediatric brain tumor autophagy and chemosensitivity. J Neurooncol 2012;106:281–90.
49. Westendorf AF, Zerzankova L, Salassa L, Sadler PJ, Brabec V, Bednarski PJ. Influence of pyridine versus piperidine ligands on the chemical, DNA binding and cytotoxic properties of light activated trans,trans,trans-[Pt$(N_3)_2(OH)_2(NH_3)(L)$]. J Inorg Biochem 2011;105: 652–62.
50. Westendorf AF, Bodtke A, Bednarski PJ. Studies on the photoactivation of two cytotoxic *trans,trans,trans*-diazidodiaminodihydroxo-Pt(IV) complexes. Dalton Trans 2011;40:5342–51.